In-situ tensile test on 316H SENT using Digital Image Correlation

Laurie Podesta, Bertrand Wattrisse, Félix Latourte, Laurent Waltz, Jean-Michel Muracciole

IN-SITU TENSILE TEST ON 316H SENT USING DIGITAL IMAGE CORRELATION

L. Podesta[1,2], B. Wattrisse[2], F. Latourte[1], L. Waltz[2] and J-M. Muracciole[2]
[1] EDF R&D, Site des Renardières, Avenue des Renardières - Ecuelles, 77818 Moret-sur-Loing, France
[2] ThM2, LMGC / CNRS / University Montpellier
163 Rue Auguste Broussonnet, 34090 Montpellier, France
Email: laurie.podesta@edf.fr

ABSTRACT

At elevated temperature (550°C) intergranular creep cracks are prone to develop in thermally and environmentally aged 316 stainless steel. To improve the understanding of mechanisms responsible of creep cracking, some micromechanical experiments have been conducted. Single Edge Notched Tensile specimens (SENT) made of 316H have been machined with a desired ratio of $a/W = 0.15$ with a the crack length and W the width specimen. After a fine polishing preparation, the samples are then thermally aged using an oxidizing treatment at 600 °C in a rich-carbon environment during 2000 hours. It has been assumed that it induces carbide precipitation at grain boundaries ($Cr_{23}C_6$) leading to a loss of corrosion resistance and to a material embrittlement. In parallel, the oxide (Fe_3O_4) layer grows at the surface up to 50 μm. Its random structure is particularly convenient as a surface marker for the Digital Image Correlation (DIC). A tensile device placed in the SEM chamber is used to apply cycles of loading/unloading to the specimen combining this with a Scanning Electron Microscope (SEM) images acquisitions of the crack tip vicinity. Complementary finite element (FE) simulations of intergranular cracks in bicrystals have been performed and used as reference fields to develop an identification procedure of the crack tip position. It relies on kinematic measurements using a local approach and on projections using Linear Elastic Fracture Mechanic (LEFM) expressions. Experimental evidences have been obtained of plasticity developing ahead of the crack when a local load is applied. A quantification of biais due to the model errors when plasticity is taken into account is done as well as an assessment of the robustness of the procedure. We propose a comparison between FE modeling and full-fields measurements resulting from an *in-situ* tensile test in a pre-cracked sample.

Keywords: Austenitic Steel, Crystal Plasticity, Digital Image Correlation, Linear Elastic Fracture Mechanic, SEM

INTRODUCTION

At high temperature one of the most detrimental damage mechanism during creep is intergranular cracking. In addition, in harsh environment (CO_2), oxygen and carbon elements diffusion along the grain boundaries is observed. To better understand the crack initiation and propagation in the aged 316H stainless steel, some experiments on microsized specimens are proposed. The creep crack monitoring during *in-situ* tests will be performed combining DIC using high resolution images acquired by microscopy and LEFM expressions. It has been shown that the Williams' series [1] and the Westergaard's solutions [2] are quite efficient to determine the stress intensity factors (SIF) [3, 4] and the crack tip position [5]. Several behaviours have been considered in the current study: elasticity, macroscopic isotropic plasticity and crystal plasticity. Here, the results related to phenomenological crystal plasticity are solely presented. The law chosen to describe the plastic response of the 316H at the grain scale was initially proposed by Méric and Cailletaud [6] and is now commonly used for cyclic loadings in austenitic stainless steels [7]. Crystal plasticity is also relevant to model crystal creep deformation, for example on Ni-based single crystals [8] or in polycrystalline Ti-based alloys such as Ta_6V [9]. In this paper, an identification procedure of the crack tip position based on kinematic measurements is presented. It is then validated on real images deformed by a known displacement field associated with the development of crack either for a linear or non-linear behavior, allowing a metrological assessment of the procedure.

MICROSAMPLE PREPARATION

The Grade 316H stainless steel material considered for testing has been in service for 98704 hours at a typical temperature of 500-520 °C. It was not exposed to carbon-rich environment. Therefore the service exposure will only have led to thermal ageing as the service stresses were too low for any significant creep deformation or damage [10]. SENT samples have been machined from this ex-service material with a desired ratio of $a/W = 0.15$ with a the crack length and W the width specimen using Electric Discharge Machining (EDM). Prior to SENT machining, CT samples are submitted to fatigue cycles to propagate a sharp crack from the notch. Then, the CT is cut into 1mm thick slices using EDM and polished up to 4000 SiC paper to allow the crack tip detection from SEM imaging. The fatigue crack path seems to be inter or transgranular (Figure 2(a)).

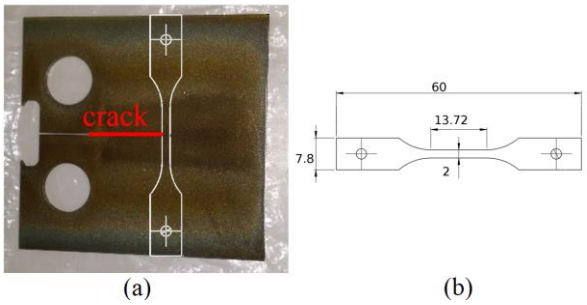

Fig. 1: Preliminary machining of pre-cracked CT sample (a) before performing the final EDM of the SENT (b)

A specific oxidizing treatment, named preconditioning, has been developed to increase the diffusion of oxygen and carbon (C, O) in a reasonable time. After a fine polishing preparation (Figure 2(a)), the samples are then submitted to preconditioning at 600 °C in CO_2 environment during 2000 hours (Figure 2(b)). In parallel, the oxide (Fe_3O_4) layer growths at the surface up to 50 µm hiding the crack that propagated during the prior fatigue load.

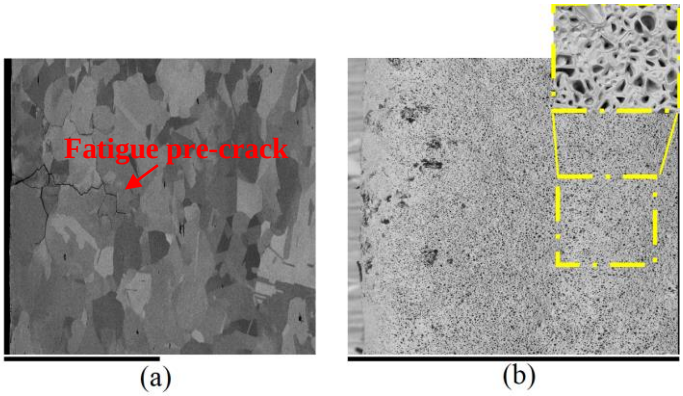

Fig. 2: Inter/trans- granular fatigue crack path appears at SENT surface after fine polishing (a) but cannot be monitored after preconditioning treatment (b). The scale bar is 500 µm and the square length is 35 µm

EXPERIMENTAL SET-UP

To monitor the crack propagation, a FEI Quanta FEG 600 SEM is used, in combination with a tensile device to apply cycles of loading/unloading. SEM images acquisitions of the crack tip vicinity are conducted. The test is performed at room temperature and vacuum. While the crack propagates, the plasticity development is determined (first step of plasticity, plastic increment, etc…). The loading level is increased as sample surface evolves. Up to loading step A (see Figure 3), no change is visible but a relaxation phenomenon appears, highlighting a viscous behavior. Then, the crack propagation is observed between loading steps 0 and 3. The force acquisition versus time is shown in Figure 3. Red dots indicate image acquisition.

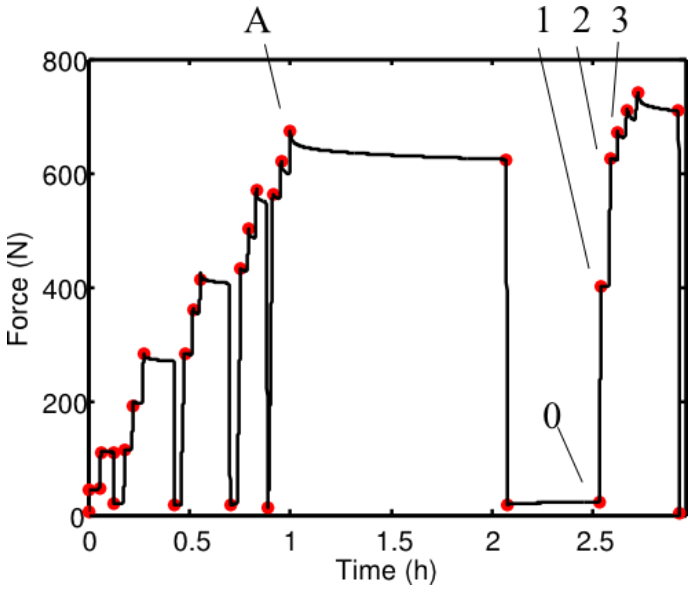

Fig. 3: Loading/unloading cycles during the *in-situ* tensile test: loading step A corresponds to the first propagation of the crack, the loading step 0 is defined as a reference state with a load of 20N allowing to image the crack tip, loading step 1 at 400N, loading step 2 at 620N and loading step 3 at 670N

KINEMATIC MEASUREMENTS USING DIGITAL IMAGE CORRELATION

Kinematic measurements are performed by Digital Image Correlation (DIC) on the surface of a polycrystal of 316H austenitic steel. DIC requires a gray level texture with a dynamic range as large as possible with local contrast variations. In the present case, the random structure of the oxide layer is particularly convenient as a surface marker. The Region Of Interest (ROI) covers a 500 µm side square surface that corresponds to 2048 pixels. Using the same apparatus, the imaging distorsions have been quantified by Guery [11] and are neglected in this work. The displacement fields are measured between two consecutive images considering a local DIC approach on a dense grid. The size of the correlation subsets was 12 pixels and the grid step was 1 pixel. Consequently, the measured displacements are not statistically independent between two adjacent points. Two mechanical quantities of interest are assessed: the oxide deformation prior to crack propagation and the crack advance considering the experimental conditions. They are determined by fitting the displacement field using a specific set of functions related to linear elastic fracture mechanics (*e.g.* Williams'series).

The chosen shape functions for the local DIC algorithm are constant so that the displacement fields obtained by DIC will not be strongly discontinuous due to the finite length scales introduces in the DIC. In other words, the displacement discontinuity due to the crack will be poorly captured.

PROJECTION ONTO LINEAR ELASTIC FRACTURE MECHANIC BASIS

Williams' series or Westergaard's solutions have been used in Fracture Mechanics to describe the kinematic response of semi-infinite structure under uniaxial loading. Williams' series are used in this work for post-processing the displacement measured by DIC. According to the LEFM theory, the displacement can be expressed, in the polar coordinates, as a combination of contribution from different orders in mode I (opening mode) or mode II (sliding mode) leading to the general equation (Equation 1). An illustration of the chosen coordinates around the crack tip is proposed in Figure 4.

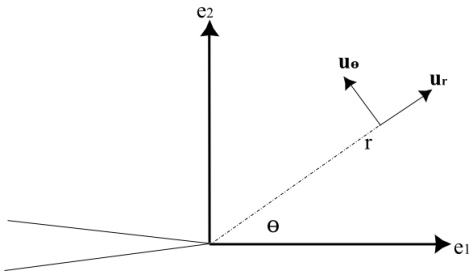

Fig. 4: Local coordinate system around the crack tip

Using these coordinates, the displacement field corresponding to the Williams' series reads:

$$u(r,\theta) = \sum_{i=I,II} \sum_{n} a_i^n \phi_i^n(r,\theta) \tag{1}$$

where *n* corresponds to the considered order, a_i^n are the target parameters and ϕ_i^n are the reference fields from LEFM, and *i* is the crack mode. The ϕ_i^n expressions must be separated in agreement with the considered mode: mode I (Equation 2), mode II (Equation 3).

$$\phi_I^n = r^{n/2}.(\kappa.e^{(jn\theta/2)} - (\frac{n}{2}).e^{(j(4-n).\theta/2)} + ((\frac{n}{2}) + (-1)^n).e^{(-jn\theta/2)}) \tag{2}$$

$$\phi_{II}^n = jr^{n/2}.(\kappa.e^{(jn\theta/2)} + (\frac{n}{2}).e^{(j(4-n).\theta/2)} - ((\frac{n}{2}) - (-1)^n).e^{(-jn\theta/2)}) \tag{3}$$

where κ is the Kolossov's constant (κ = (3-υ)/(1+υ) in the stress plane conditions, with υ the Poisson coefficient). The different orders are precised in Table 1.

order	n <0	n = 0	n = 1	n = 2
Designation and mechanical use	Supersingular	Rigid body translation	SIF	Uniform T-stress and both rotation

Tab. 1: Denomination attributed to each Williams' series orders

In this work, we have chosen to project the displacement fields measured by DIC on a specific set of Williams' series restricted to a mode I crack, using orders 0, 1 and 2.

SIMULATION USING A CRYSTAL PLASTICITY MODEL

The simulation of the experimental tensile test is performed using the finite element software Code_Aster. The phenomenological crystal plasticity law proposed by Méric and Cailletaud [6] has been chosen in this study. Intergranular cracked bicrystal has been modeling and meshed using quadratic quadrangles (Figure 5(a)) using the Salome software. To provide numerical convergence, the crack is modelled as a notch of very small radius. A mesh refinement in the notch tip region has been performed (Figure 5(b)). The crack position is perfectly known. Two boundaries conditions can be used to load the structure: Westergaard's solutions in displacement prescribed for the global boundary, or imposed displacement on the upper and lower boundaries while the lateral ones are stress-free. It is important to note that this latest case (material properties and boundary conditions) are not consistent with the analytic solutions given by the Williams's series. The crystal plasticity response considering Westergaard's boundaries conditions is solely presented here. Because of the non-dimensional nature of the problem, the width and height of the simulation box are taken equal to 1.

Considering a Face Centered Cubic (FCC) crystals, numerous misorientations have been studied but only one bicrystal example will be presented. The material parameters correspond to a 316L polycrystalline aggregate [7]. The displacement fields corresponding to this numerical study are shown in Figure 6. The fields computed by Code Aster are shown in Figure 6a and 6c. From these reference solutions, a projection was done using the chosen Williams' series, for an imposed position of the crack tip. The projected fields are shown in Figure 6b and 6d. The mismatch between the reference fields and the projected ones is attributed to plasticity. Finally, a complete identification of crack parameters (crack position and angle and Williams' series coefficients) has been conducted for different initial guesses of crack tip position, and the results are provided in Table 2.

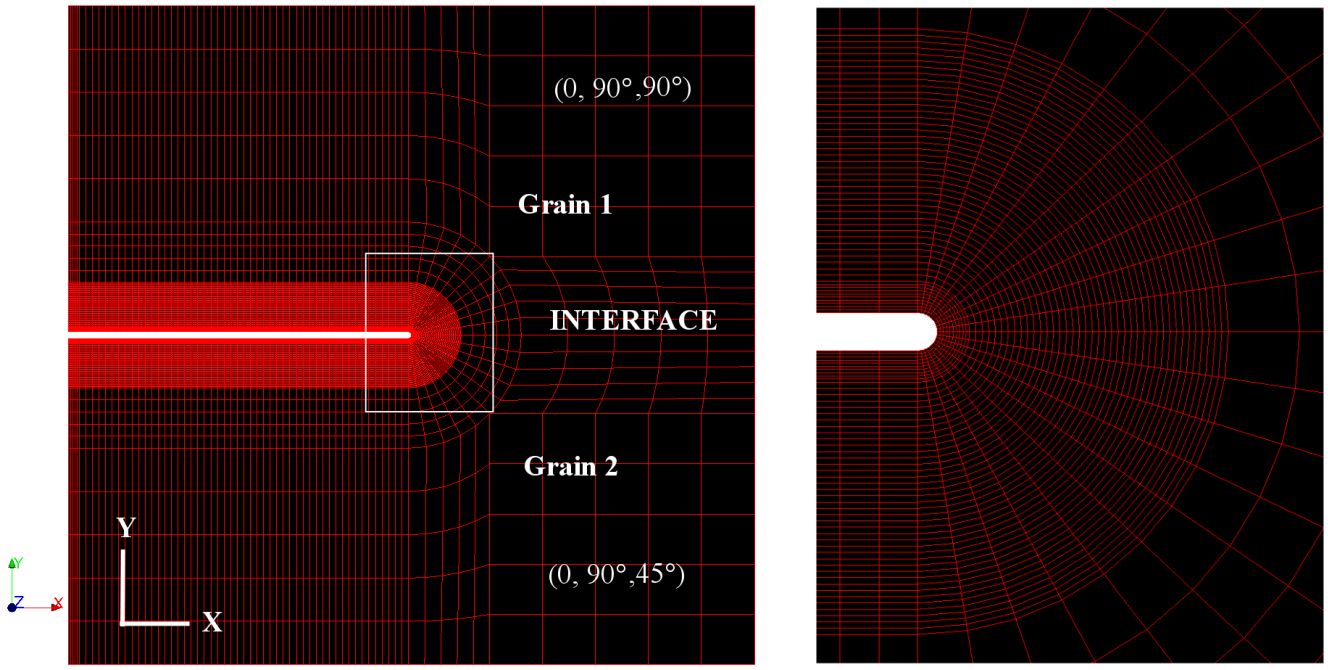

Fig. 5: Cracked bicrystal mesh (7850 faces and 23951 nodes)

The adimensional positions appearing in Table 2 are defined as:

$$\hat{x} = \frac{x}{L_x} \tag{4}$$

$$\hat{y} = \frac{y}{L_y} \tag{5}$$

with L_x and L_y the investigated area dimensions in the two directions.

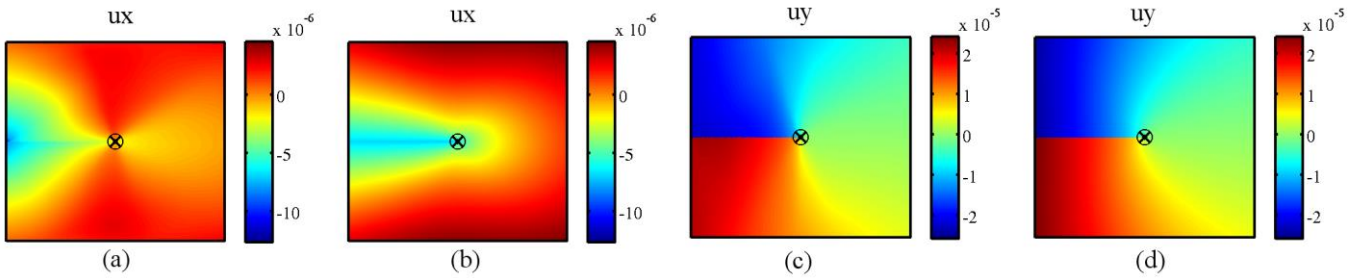

Fig. 6: Comparisons between the kinematic fields computed by FE analysis corresponding to Westergaard's boundary conditions (component u_x(a) and u_y(c)) and the optimized displacement fields from Williams' series provided by Equations 1, 2 and 3 (component u_x(b) and u_y(d))

	$\hat{x}$	$\hat{y}$	**Θ (radian)**	a_1^I **(MPa.√m)**
Initial	**0**	**0**	**0**	**0.01**
Optimized	**$-6.9.10^{-4}$**	**$5.1.10^{-4}$**	**$-7.02.10^{-5}$**	**0.015**
Initial	**0.05**	**0.05**	**0.035**	**0.01**
Optimized	**$1.6.10^{-2}$**	**$1.2.10^{-3}$**	**$1.00.10^{-2}$**	**0.012**

Tab. 2: Comparisons between estimated values and the optimized crack tip position and Williams' coefficient

ASSESSMENT OF THE IDENTIFICATION PROCEDURE: THE EXPERIMENTAL TEST

During the *in-situ* tensile test, the crack propagation in the oxide layer is observed (Figure 7). The Williams' series are not linear with respect to the crack tip position. Consequently, an estimation of the crack tip position has to be introduced in the identification procedure. Here, the crack tip is arbitrarily supposed to be located close to the image center. This estimation can be improved when a crack is visible in the SEM images.

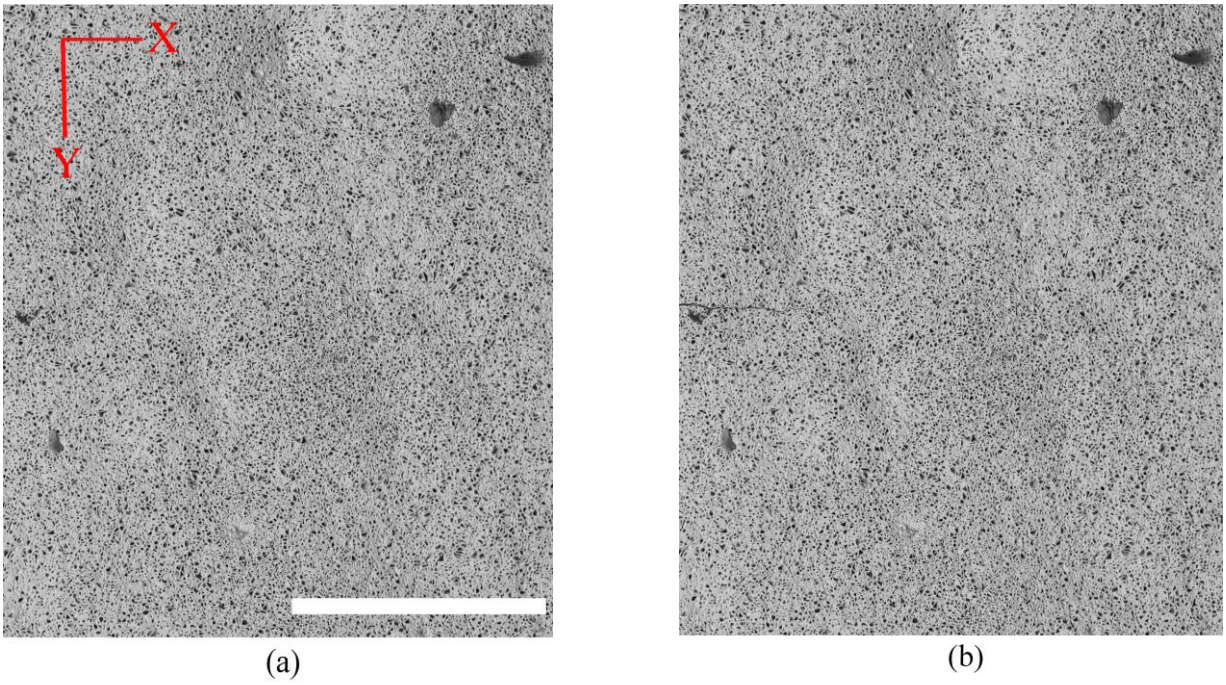

Fig. 7: SEM images of the reference state for loading step 0 (a) and after propagation for loading step 2 (F = 620N) (b). The physical size of the pixels is 0.244 µm. The scale bar is 250µm

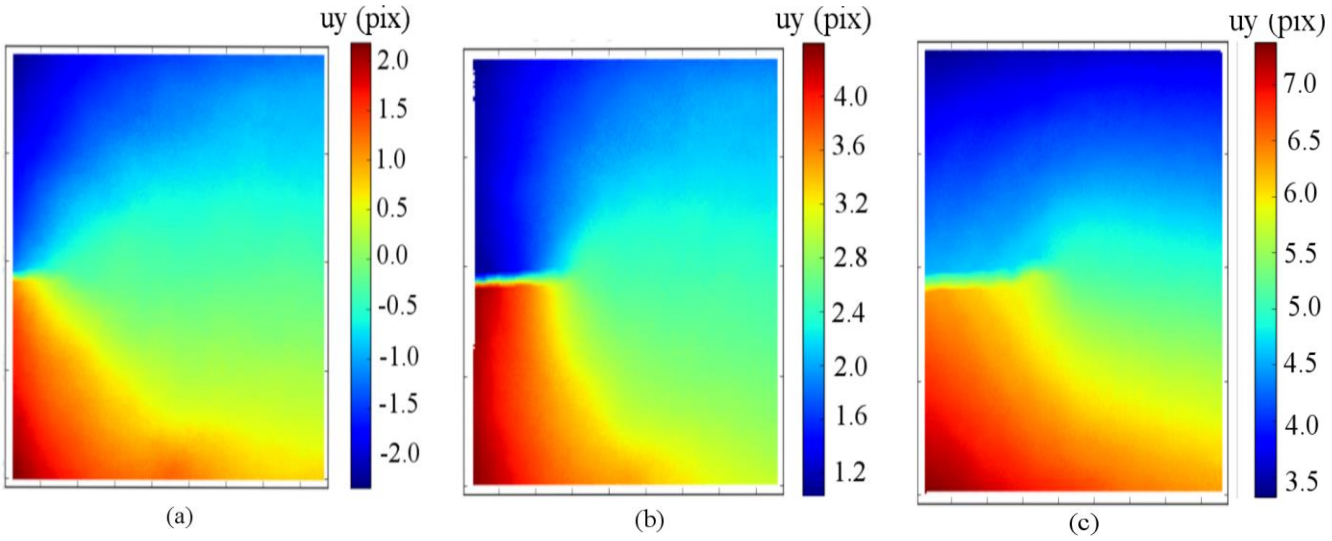

Fig. 8: Displacement fields obtained by DIC u_y for loading step 1 at 400N (a), step 2 at 620N (b) and step 3 at 670N (c)

Considering the crack tip position estimation and the Williams' series expressions, a comparison between the DIC results (Figure 8) and the analytical displacement fields can be performed. Then, a least square minimization is used to identify the crack tip parameters and the Williams' series coefficients. The results from the optimization is given in the Figure 9. A black circle is used as marker for the optimized crack tip position.

The residuals map shown a good agreement between the reference image and the deformed image corrected by the displacement for the DIC results and the analytical expressions (Figure 10). The Table 3 summarizes the results of crack parameters identification. The physical size of the pixel is 0.24µm. The scale bar is 250µm (1000 pixels).

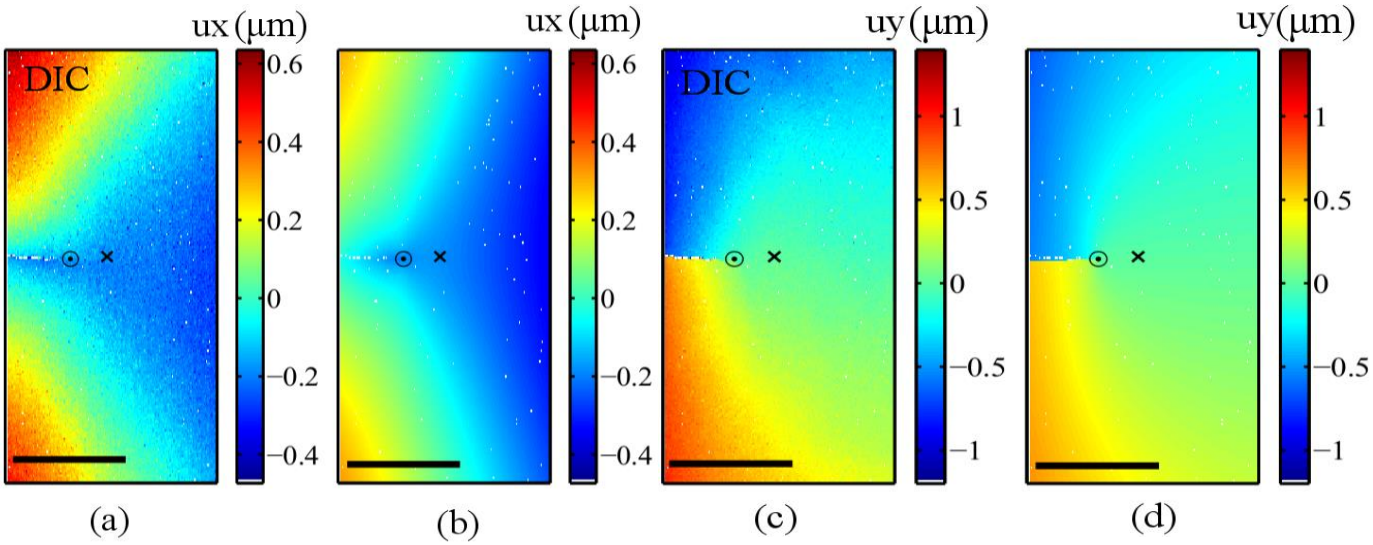

Fig. 9: Comparisons between the kinematic fields obtained by DIC (component u_x(a) and u_y(c)) and the optimized Williams' displacement fields (component u_x(b) and u_y(d)) for F = 620N

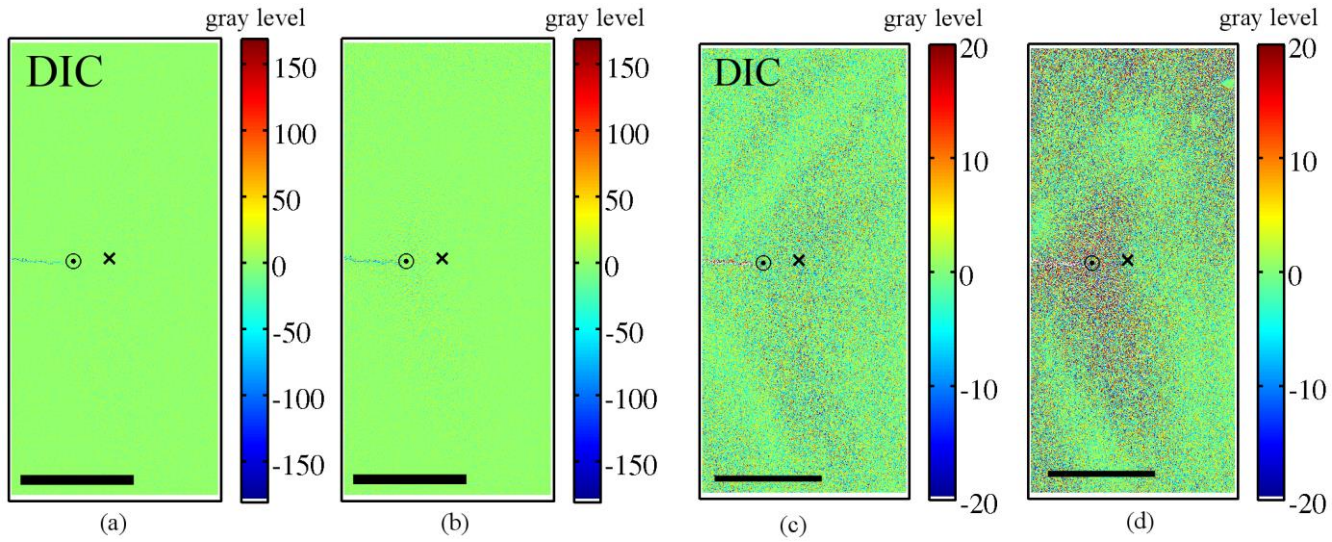

Fig. 10: Residual maps for the DIC ((a),(c)) and the Williams'expressions ((b),(d)) with a thresholded colorbar of values ((c),(d)) to highlight the low values of residuals (F = 620N). The colorbars correspond to gray levels coded in 8 bits

A quantitative assessment of the results is presented in Table 3. The bold values of x_0 highlight the crack propagation as a function of increasing load. For step 2 and 3 at loads of 620N and 670N, a same initial guess was chosen for the crack tip position that was not detrimental to capture the crack propagation.

	x_0 (pixel)	y_0 (pixel)	Θ (radian)	Force (N)
Initial	291	1057	0.00	400
Optimized	**240.1**	981.0	7.0010^{-5}	
Initial	835	975	0.00	620
Optimized	**535.6**	986.0	$-2.169.10^{-2}$	
Initial	835	975	0.00	670
Optimized	**651.7**	1048.5	$-2.2661.10^{-2}$	

Tab. 3: Comparisons between estimated values and the optimized crack tip position

CONCLUSIONS

At elevated temperature (550°C) intergranular creep cracks have been observed in thermally and environmentally aged 316 stainless steel. To improve the understanding of mechanisms responsible of creep cracking, some micromechanical experiments have been conducted. Single Edge Notched Tensile specimens (SENT) made of 316H have been machined with a desired ratio of $a/W = 0.15$ with a the crack length and W the width specimen. A tensile device placed in the SEM chamber is used to apply cycles of loading/unloading to the specimen combining this with a Scanning Electron Microscope (SEM) images acquisitions of the crack tip vicinity. Complementary finite element (FE) simulations of intergranular cracks in bicrystals have been performed and used as reference fields to develop an identification procedure of the crack tip position. It relies on kinematic measurements using a local DIC approach and on projections using Linear Elastic Fracture Mechanic (LEFM) expressions. Experimental evidences have been obtained of plasticity developing ahead of the crack when a local load is applied. A quantification of bias due to the model errors when plasticity is taken into account is possible as well as the robustness of the procedure. We propose a comparison between FE modeling and full-fields measurements resulting from an *in-situ* tensile test in a pre-cracked sample. This procedure will be applied to creep loaded specimens.

REFERENCES

[1] Williams M.L., On the stress distribution at the base of a stationary crack. *Journal of Applied Mechanics*, 24, 109-114, 1957

[2] Westergaard H., Bearing pressure and cracks. *Journal of Applied Mechanics*, 6, 49-553, 1939.

[3] Roux-Langlois C., Gravouil A., Baietto M-C., Réthoré J., Mathieu F., Hild F. and Roux S., DIC identification and X-FEM simulation of fatigue crack growth based on the Williams'series. *International Journal of Solids and Structures*, 53, 38-47, 2015

[4] Pataky GJ., Sangid MD., Sehitoglu H., Hamilton RF., Maier HJ. And Sofronis P, Full field measurements of anisotropic stress intensity factor ranges in fatigue. *Engineering Fracture Mechanics*, 94, 13-28, 2012.

[5] Réthoré J., Roux S. and Hild, F., Optimal and noise-robust extraction of Fracture Mechanics parameters from kinematic measurements. *Engineering Fracture Mechanics*, 78, 1827-1845, 2011.

[6] Méric L., Poubanne P. and Cailletaud G., Single crystal modeling for structural calculations: Part 1 – Model Presentation. *Journal of engineering materials and technology transaction of the ASME*, 113, 162-170, 1991.

[7] Guilhem Y., Basseville S., Curtit F., Stephan J-M. and Cailletaud G., Numerical investigations of the free surface effect in threee dimensional polycristalline aggregates. *Computational Materials Science*, 70, 150-162, 2013.

[8] Samal M.K. and Ghosh S., Evaluation of creep deformation and mechanical properties of Nickel-based superalloys through FE analysis based on crystal plasticity models. *Proc. Engineering*, 55, 342-347, 2013.

[9] Hasija V., Ghosh S., Mills M.J. and Joseph, D.S., Deformation and creep modeling in polycrystalline Ta_6Al alloys. *Acta Materialia*, 51, 4533-4549, 2003.

[10] Chevalier M., Impact of in-service carburization on the creep-fatigue lifetime of stainless steel components and suggested assessment procedure modifications. Creep Conference, 2015.

[11] Guery A., Latourte F., Hild F., and Roux S., Characterization of SEM speckle pattern marking and imaging distortion by digital image correlation. *Measurement Science and Technology*, 25, 015401, 2014.